Electrocatalysis (2014) 5:41–49
DOI 10.1007/s12678-013-0162-1

$NiMnO_x$/C: A Non-noble Ethanol-Tolerant Catalyst for Oxygen Reduction in Alkaline Exchange Membrane DEFC

Amanda C. Garcia · Jose J. Linares · Marian Chatenet · Edson A. Ticianelli

Published online: 27 September 2013

Abstract A non-noble oxygen reduction catalyst based on nickel–manganese oxide supported on high-surface area carbon has been synthesized by a mild hydrothermal treatment, resulting in nanocrystalline needles. Cyclic voltammetry showed the electrochemical redox characteristics of this material, evidencing the appearance of peaks associated to consecutive reversible transitions involving Mn(IV)/Mn(III) and Mn(III)/Mn(II). The catalyst displayed a high activity for the oxygen reduction, despite that the complete reduction was not achieved, consuming less than three electrons of the four available in the oxygen molecule. More importantly, this activity did not decay under the presence of ethanol, revealing the high ethanol tolerance of this material. Finally, single-cell results have demonstrated the suitability of this material as cathode catalysts for alkaline DEFC: The open circuit voltage and the maximum power densities are close to those obtained by a standard Pt/C catalyst.

Keywords Alkaline direct ethanol fuel cell · Ethanol tolerance · Oxygen reduction reaction · Nickel-doped manganese oxides

A. C. Garcia (✉) · E. A. Ticianelli
Instituto de Química de São Carlos, Universidade de São Paulo, CP 780, 13560-970 São Carlos, São Paulo, Brazil
e-mail: amandagarcia@iqsc.usp.br

J. J. Linares
Instituto de Química, Universidade de Brasília, CP 4478, 70910-000 Brasília, Distrito Federal, Brazil

M. Chatenet
Laboratoire d'Electrochimie et de Physico-chimie des Matériaux et des Interfaces LEPMI, UMR 5279 CNRS/Grenoble-INP/Université de Savoie/Université Joseph Fourier, BP 75, 38402 Saint Martin d'Hères, Cedex, France

Introduction

The oxygen reduction and ethanol oxidation reactions on platinum-based electrodes have been extensively investigated since low-temperature direct ethanol fuel cells (DEFCs) offer a promising method of electric energy production [1–3]. Ethanol has a higher energy density than methanol (8.0 versus 6.1 kW kg^{-1}), which implies more energy available from this fuel when used, for example, in portable applications [4]. Notwithstanding, it is well known that DEFC undergoes undesirable process such as the poisoning of the cathode surface due to the fuel crossover through the membrane [5]. This may lead to a mixed potential, as a consequence of the simultaneous oxygen reduction reaction (ORR) and ethanol oxidation reaction in the cathode, which causes the cathode depolarization and overall depresses the cell efficiency. Pt-based catalysts dispersed on a carbon support, although well-known active catalysts for the ORR are also good promoters of the electro-oxidation of small organic molecules, which typically gives rise to competition between the alcohol molecules and the oxygen species for the platinum active sites in case of significant fuel crossover, thereby ruining the cathode ORR activity.

The development of membranes [6, 7] that inhibit the crossover of alcohol and the design of cathodes tolerant to ethanol are two strategies normally employed to overcome this problem [8, 9]. In the search for ethanol-tolerant catalysts, several Pt-based materials have been recently postulated as promising ones, both in alkaline and acidic media. However, platinum presents some drawbacks that offset its full development: gradual decrease of the activity with time, ascribed to degradation process (agglomeration and dissolution processes) [10, 11], and, from a market

point of view, it is an expensive material with, up to now, limited availability [12, 13]. In order to overcome these limitations, Pt-free catalysts have focused the attention of the scientific community, with significant recent development in materials such as manganese oxide (MnO_x)-based electrocatalysts [14–17].

In this context, this paper describes the results related to the synthesis, characterization, and applications of a nanometric $NiMnO_x$/C material in alkaline medium as an ethanol-tolerant ORR electrocatalyst. The prepared material was first structurally investigated, by X-ray diffraction (XRD) and high-resolution transmission electron microscopy (HRTEM), in order to characterize the nature of the nanocrystalline phase(s) and the nanostructure arrangement of the $NiMnO_x$/C nanocrystallites. Fundamental electrochemical measurements were then performed in order to primarily understand the oxygen reduction mechanism and kinetics on this material, both in the absence and presence of ethanol. Specific studies were conducted with the aim of assessing the ethanol tolerance of $NiMnO_x$/C cathodes. To reach this goal, the $NiMnO_x$/C was implemented as cathode catalyst in an alkaline DEFC, and the single cell performance was evaluated, in comparison to a standard Pt/C catalyzed-cathode (20 wt% Pt/Vulcan XC72 from E-Tek).

Experimental

Synthesis and Physicochemical Characterizations of the MnOx/C-based Catalyst

Nickel-doped manganese oxide dispersed onto E350 carbon (from Timcal) was prepared by a mild hydrothermal treatment first described by Bezdicka et al. [18]. More specifically, the $NiMnO_x$/C material was obtained by suspending the desired amount of the carbon black powder in an aqueous solution of $MnSO_4$ (Merck) and $Ni(NO_3)_2{\cdot}6H_2O$ (Merck®), in which $KMnO_4$ was added to reach the targeted Mn loading (ca. 20 wt%). The suspension was maintained at a controlled temperature 80 °C for 15 min, and then the $NiMnO_x$/C was filtered and dried at 110 °C.

The Ni-doped MnO_x/C electrocatalyst was characterized using XRD analyses conducted on a Philips TW 1730 vertical goniometer/diffractometer equipped with a diffracted-beam monochromator, using Fe K_α radiation. The discrete particle morphology, shape, and Ni/Mn ratio distribution were investigated using HRTEM conducted on a JEOL 2010 equipment baring an energy dispersive X-ray spectrometer for chemical analyses. For this, the electron beam was lowered down to nanometric size, in order to monitor only the fluorescence of the desired area of the sample. These results were thoroughly discussed in a previous paper [19].

Fundamental Electrochemical Tests

Preparation of the Electrode

In order to characterize the voltammetric redox activity of the catalysts, a thin layer of the material was deposited on a glassy carbon disk of 0.5 cm of diameter, corresponding to a geometric area of 0.196 cm^2 [20]. For the preparation of the layer, a catalytic suspension of 2.0 mg of $NiMnO_x$/C powder, 1 mL isopropyl alcohol, and 20 μL of 5 wt% Nafion® was mixed and ultrasonically homogenized. Afterwards, 20 μL of the obtained ink were deposited on the glassy carbon electrode. The solvents were left to evaporate at room temperature, checking the homogeneity of the deposited layer with the aid of an optical microscope. For comparison purposes, a Pt/C-based (commercial 20 % Pt on Vulcan carbon black: XC-72R, BASF Fuel Cells, former E-TEK Inc.) thin-layer electrode was also prepared following the same procedure.

Electrochemical Characterization of the Carbon-Supported MnO_x/C-based Materials

All the fundamental measurements were carried out in Milli-Q water (Millipore), using 1.0 M NaOH (Merck, Suprapur) as support electrolyte. When required, 0.1 M ethanol (Merck, Suprapur) was added to the electrochemical medium. The experiments were controlled using a potentiostat/galvanostat AUTOLAB PGSTAT 20 (Ecochemie) in a three-electrode cell. The reference electrode was Hg/HgO in 1.0 M NaOH, the potential of which is +0.10 V on the normal hydrogen electrode scale.

The cyclic voltammetry experiment was carried out, sweeping the working electrode potential between −0.9 and 0.5 V versus Hg/HgO at a scan rate of 10 mV s^{-1}. Oxygen was removed from the solution by bubbling argon for 30 min. Afterwards, several cycles were repeated until obtaining a stable voltammogram. Measurements were carried out in the presence and absence of ethanol. Oxygen reduction voltammetry experiments were performed after oxygen saturation of the electrolyte during 40 min by intense bubbling previous to the measurement. Once this time elapsed, bubbling was reduced in order to perform the measurement and maintain the saturation of the solution. The ORR voltammograms were recorded at 10 mV s^{-1} from 0.2 to −0.7 V versus Hg/HgO using a rotating disk electrode (RDE), with the revolution speed ranging between Ω=100 and Ω=2,500 rpm. Prior to each experiment, the potential was kept for 2 min at the starting potential, 0.2 versus Hg/HgO in order to avoid large double-layer charging currents in all experiments.

The overall number of electrons exchanged per oxygen molecule (n) was determined from the limiting current

density plateaus, using the classical Levich equation [21] (Eq. 1).

$$j_{lim} = 0.620nFD^{2/3}C^{*}\upsilon^{-1/6}\Omega^{1/2} \quad (1)$$

The parameter j_{lim} (amperes per square meter) is the limiting current density of the polarization curves, n is the number of electrons involved in the reaction, D is the oxygen diffusion coefficient, C^* is the oxygen solubility in the solution, ν is the solution kinematic viscosity, and Ω (radians per second) is the RDE revolution speed. Available data for D, C^*, and ν in the literature are scarce for temperatures other than 25 °C. In the case of the solubility of oxygen in 1 mol L^{-1} NaOH at different temperatures, Hiemke [22] reported the values expressed in terms of the Ostwald coefficient (L, Eq. 2), where c_G is the gas concentration in the gas phase, and c_L is the gas concentration in the liquid phase (solubility).

$$L = \frac{c_L}{c_G} \quad (2)$$

Gas concentration can be calculated from the ideal gases equation of state (Eq. 3), where c_G is the concentration, P is the partial pressure of oxygen (101.3 KPa), R is the universal gas constant (8.314 J mol^{-1} K^{-1}), and T is the temperature.

$$c_G = \frac{P}{RT} \quad (3)$$

Approximate values of the Ostwald coefficient are collected in Table 1 [22] at the approximate temperatures of 290, 300, 310, and 375 K. The obtained values were fitted to the Arrhenius equation, allowing the estimation of the values at different temperatures.

$$c_L = A \cdot exp\left(\frac{B}{T}\right) \quad (4)$$

The parameter c_L is the oxygen solubility, A is a pre-exponential factor, and B is the apparent activation energy. Values of the corresponding parameters after fitting the data collected in Table 1 are 0.1832 mol m^{-3} for A and 849.52 K for B. With this, the corresponding values of the oxygen solubility at 25, 40, and 60 °C are 3.16, 2.76, and 2.35 mol m^{-3}, respectively, in reasonable agreement with the corresponding values reported in references [23, 24].

As far as we know, there are no available data for oxygen diffusivity in 1.0 mol L^{-1} NaOH at different temperatures. Chatenet et al. [23, 24] reported a value of the oxygen diffusion coefficient of $1.56 \cdot 10^{-5}$ cm^2 s^{-1} in 1.0 mol L^{-1} NaOH at 25 °C and values of $3.10 \cdot 10^{-6}$ cm^{-2} s^{-1} and $2.54 \cdot 10^{-5}$ cm^2 s^{-1} in 11.1 mol L^{-1} NaOH at 25 °C and 80 °C, respectively. The corresponding values for water at different temperatures are $1.97 \cdot 10^{-5}$ cm^2 s^{-1}, $3.24 \cdot 10^{-5}$ cm^2 s^{-1}, $3.99 \cdot 10^{-5}$ cm^2 s^{-1}, and $4.82 \cdot 10^{-5}$ cm^2 s^{-1} at 20, 40, 50, and 60 °C, respectively [25]. The value of the diffusion coefficient for 1.0 mol L^{-1} NaOH at 25 °C resembles more that of pure water rather than 11.1 mol L^{-1} NaOH. Authors consider that a rough estimation of this parameter can be obtained from the B parameter similar to Eq. 4 after fitting the oxygen diffusion coefficient in water versus temperature to the Arrhenius equation. Afterwards, by using the diffusion coefficient of O_2 in 1.0 mol L^{-1} NaOH, the pre-exponential factor (A) can be estimated. This makes possible the estimation of the oxygen diffusion coefficient in 1.0 mol L^{-1} NaOH at the different temperatures. The corresponding estimated values at 40 and 60 °C are $2.22 \cdot 10^{-5}$ cm^2 s^{-1} and $3.38 \cdot 10^{-5}$ cm^2 s^{-1}, respectively.

Finally, values of kinematic viscosities are available in Chatenet et al. [26]. The reported values at 16, 25, and 40 °C are 0.0132 cm^2 s^{-1}, 0.0104 cm^2 s^{-1}, and 0.0075 cm^2 s^{-1}. In order to estimate the value at 60 °C, it is possible to fit the experimental data to an Arrhenius type equation in the same form than Eq. 4. The value of A was $8.4529 \cdot 10^{-6}$ cm^2 s^{-1}, whereas B has a value of 2,124.5 K. With this, the extrapolated value of the kinematic viscosity at 60 °C resulted in 0.0050 cm^2 s^{-1}.

Table 1 Values of the oxygen solubility (C^*) at different temperatures from the estimation of the values of the Ostwald coefficient at different temperatures [22]

Temperature/K	c_G/mol m^{-3} (Eq. 3)	L	$c_L=C^*$/mol m^{-3} (Eq. 2)
290	42.0	0.085	3.57
300	40.6	0.075	3.05
310	39.3	0.070	2.75
375	32.5	0.055	1.79

Single-Cell Tests

The cathode catalyst was also tested in a single cell. Standard gas diffusion electrodes (GDE) were prepared with a diffusion layer formed by applying a mixture of carbon powder (Vulcan XC-72R, Cabot) with 15 % (*w/w*) of polytetrafluorethylene (PTFE, TE-306, DuPont) onto both faces of a carbon cloth substrate (PWB-3, Stackpole), using a loading (carbon+PTFE) of 3 mg cm^{-2} per side. The catalytic layer was prepared as follows. In the case of the cathode, a homogeneous suspension composed of 0.35 mL of a Nafion® solution (Aldrich, 5 wt%), 46.2 mg of $NiMnO_x$/C or Pt/C ($NiMnO_x$ or Pt basis, corresponding to 2 mg cm^{-2} of these elements in the cathode), and 0.2 mL of isopropanol was homogenized in an ultrasonic bath for 10 min, and then the solvent was completely evaporated. For the anode, the catalyst used was commercial 20 % Pt_1Ru_1 on Vulcan XC-72R (BASF Fuel Cells, former E-TEK

Inc.). The catalytic ink was prepared by mixing 34.7 mg of PtRu/C (metal basis, corresponding to 1.5 mg cm^{-2} in the anode) electrocatalysts, 0.26 mL of the Nafion® solution, and 0.15 mL of isopropanol, following the same procedure as in the case of the cathode. The resulting solid material was dispersed again in isopropanol to produce a thick ink that was quantitatively deposited by brushing on one of the faces of the composite diffusion layer of the electrode. The membrane and electrodes assemblies were prepared by sandwiching a piece of a PBI membrane, previously impregnated in KOH 6 M during 1 week, between the two electrodes. The compression pressure applied to the cell was sufficient for adhesion of the electrodes and the membrane.

High-density carbon plates with machined serpentine-type gas distribution channels were used as flow-field plates, with aluminum end plates. Voltage probes were drilled in the carbon plates, whereas current collectors were placed in the aluminum ones. Compressible carbon sheets were used between the two plates in order to ensure a good electrical contact. A thermocouple was inserted in the cathode carbon flow-field plate, coupled to a temperature controller. The system was heated with four resistances placed into the aluminum plates. The geometric area of the electrodes was 4.62 cm^2.

Measurements were carried out with a potentiostat/galvanostat AUTOLAB PGSTAT 30. The polarization curves were obtained under potentiostatic conditions from the open circuit voltage down to 200 mV, allowing the system to reach a stable current density for each voltage. Three curves were plotted each time and employed for calculating average values of current density versus potential. The operating temperatures were T=30, 45, 60, 75, and 90 °C. The fuel alkaline solution was 2 mol L^{-1} ethanol and 3 mol L^{-1} KOH. The fuel flow was 1 mL min^{-1}, with an oxygen flow rate of 100 mL min^{-1}.

Results and Discussion

Morphological Characterizations of the $NiMnO_x$/C-based Catalysts

Figure 1 displays the XRD profile for the $NiMnO_x$/C catalyst. It is observed that the diffractogram is relatively complex and involves several peaks associated to different crystalline orientation phases [19]. According to the literature, and on the basis of the most probable present species, several peaks can be tentatively identified [27–30]: The peak located at approximately 28° can be ascribed to MnO_2 (1 1 0), with a tiny shoulder at 23° associated to Mn_2O_3 (2 1 1). The presence of a small peak at 33° is also associated to Mn_2O_3 (2 2 2). Two almost overlapped peaks appear around 38°, which can be ascribed to MnO_2 (1 0 1) and to the presence of NiO (1 1 1). Afterwards, there are two new consecutive peaks around 42°: MnO_2 (2 0 0) and NiO (2 0 0), respectively. Also, two very small peaks

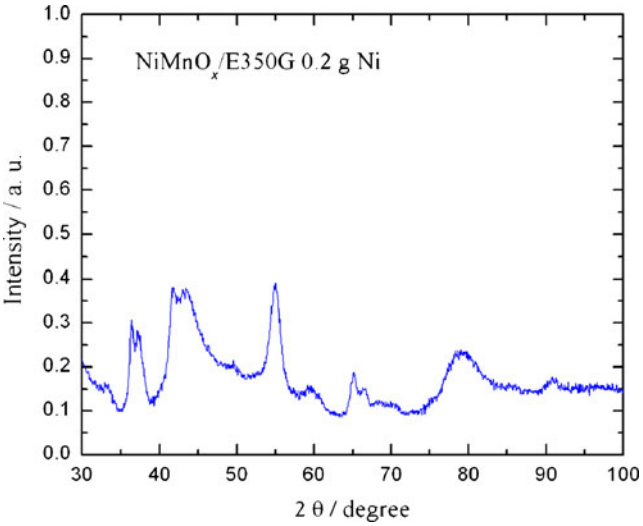

Fig. 1 DRX pattern of the synthesized $NiMnO_x$/C catalyst

appear around 45 and 50°, which can be ascribed to a reduced presence of metallic Ni (1 1 1) and (2 0 0), respectively. Therefore, several species may be present in the catalyst, and, as seen below, they are responsible for the electrochemical activity of this material.

Figure 2 shows HRTEM images for the $NiMnO_x$/C catalyst. An outstanding feature of this material is the particular shape of the deposited $NiMnO_x$ species on the carbon support, in the form of needles (Fig. 2a). Figure 2b presents a higher-resolution image, showing that the structures of the Mn oxide phases are highly monocrystalline, with several surface orientations. From these TEM analyses, it is estimated that the nanocrystalline needles exhibit diameters of the order of 5 nm and lengths close to 100 nm. These features have been previously reported for such a material [19] and rely on the preparation procedure of the catalyst. This is important since its oxygen reduction activity depends on the morphology, as well as on the composition of the $NiMnO_x$/C nanocrystallites [17, 19, 31–33]. According to previous results [19] with respect to the activity of different $NiMnO_x$ structures toward O_2 reduction, it was found that the most effective electrocatalyst is the nanostructure formed by highly oriented needles, probably because the needles have a higher Ni content and the HO^-_2 disproportionation reaction progressively increases with the Ni content in NiMnO*x* materials. Consequently, the catalyst supported on the E350G carbon promotes faster disproportionation reaction, thus leading to an overall four-electron ORR pathway. Finally, the $NiMnO_x$/C was determined to be approximately 20 %, with a nickel percentage of 0.3 and a Mn percentage of 12.8 [17].

Electrochemical Characterization of $NiMnO_x$/C Catalyst for Oxygen Reduction

Figure 3 displays the cyclic voltammogram profiles of the $NiMnO_x$/E350 (0.2 g of Ni) in O_2-free 1.0 mol L^{-1} NaOH

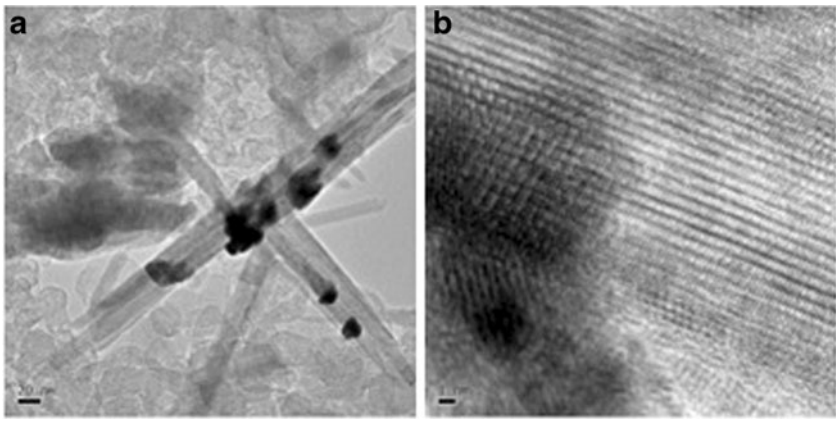

Fig. 2 **a** TEM and **b** high-resolution TEM images of the $NiMnO_x$/C catalyst

solution in the absence and presence of ethanol at a scan rate of 10.0 mV s^{-1}, at different temperatures. The peaks in the voltammograms can be referred to the consecutive redox pairs involving Mn(II)/Mn(III) (E = −0.05 V versus Hg/HgO) and Mn(III)/Mn(IV) (E = −0.3 V versus Hg/HgO) species. More importantly, the voltammograms reflect that the presence of ethanol hardly affects its baseline shape, even when operating at 60 °C. This is clearly a first indication of a suitable ethanol-tolerant catalyst. The small decrease observed in the values of the current density can be attributed to a minimal poisoning effect of some ethanol molecules adsorbed on the catalyst active sites.

Despite this promising result, evidences for a suitable ethanol-tolerant cathode catalyst have to be drawn from the actual performance for the oxygen reduction reaction (ORR). Figure 4 collects the corresponding ORR performances in a RDE at different rotation speeds, in the absence and presence (0.1 M) of ethanol at 25, 40, and 60 °C. Independently of the presence of ethanol, classical diffusion–convection plateaus

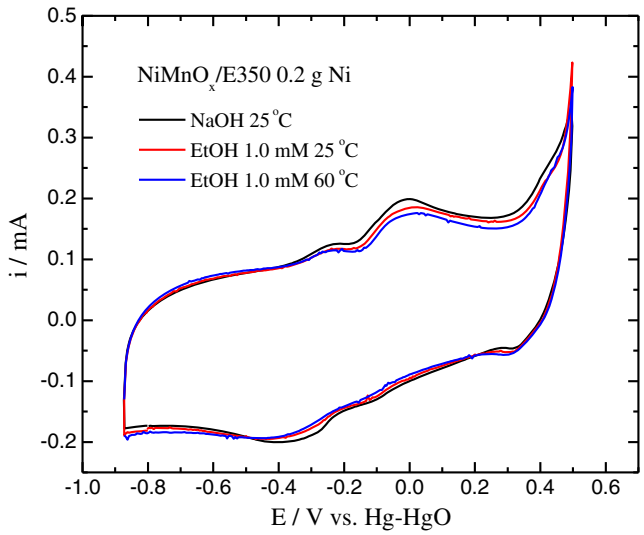

Fig. 3 Cyclic voltammograms for $NiMnO_x$/C catalyst obtained at 0.01 V s^{-1} in 1.0 mol L^{-1} NaOH and 0.1 mol L^{-1} ethanol at different temperatures

are observed. From this particular region, it is possible to assess the number of electrons involved per oxygen molecule by applying Eq. 1. The corresponding values of limiting current and number of electrons are collected in Table 2 for all temperatures. For comparison purposes, the values corresponding to Pt/C are also collected (curves not shown), also serving as reference, since a number of exchanged electrons of four should be expected. Values of the onset potentials are not collected because they do not significantly change with the temperature, all of them being in a narrow range of potential around −0.002 V versus Hg/HgO.

Pt/C in alkaline medium shows a virtually complete O_2 reduction, consuming the four electrons available per oxygen molecule at 25 and 40 °C, as expected. At 60 °C, this value drops to 3.4 e^-. In the case of the $NiMnO_x$/C, the number of electrons involved is smaller, indicative of an incomplete oxygen reduction that yields peroxide ions (HO_2^-). Manganese oxide is known to be partially effective for oxygen reduction in alkaline medium (n close to 2), due to a disfavored disproportionation of this HO_2^- species [34]. Nickel is known to increase the efficiency of the oxygen reduction reaction in alkaline medium [19, 35], and indeed, the $NiMnO_x$/C displays a value of n equal to 3. With the increase of the temperature, there is a drop in the number of electrons, from 2.8 at 40 °C to 2.5 at 60 °C. Roche and Scott [36] reported a similar behavior for manganese oxide, indicating that the temperature seems to favor the generation of the undesirable peroxide species. It is likely that the carbon substrate of the manganese oxide nanoparticles contributes to a larger extent to the overall ORR current at higher temperature, carbon being a promoter of the two-electron pathway [37].

Figure 4 also compares the polarization responses toward the ORR in the presence of 0.1 M ethanol in alkaline solution at 25, 40, and 60 °C (colored traces). As it can be observed, the electrocatalyst is tolerant to the presence of 0.1 M ethanol: The presence of the alcohol leads to a slight decrease in the values of the limiting current densities and hence, in the number of electrons exchanged per O_2 species (see Table 2). The absence of activity for ethanol oxidation (Fig. 3) may indicate that the

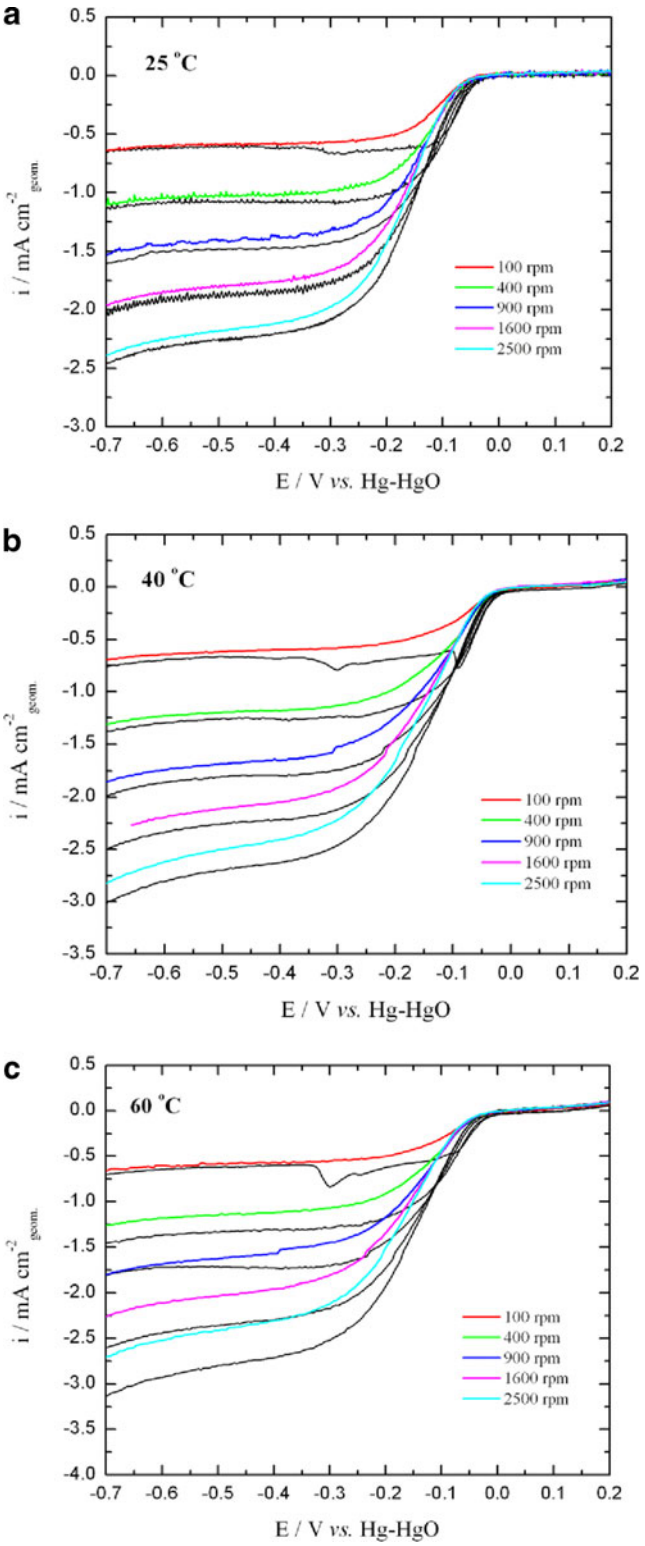

Fig. 4 Voltammograms toward oxygen reduction reaction $NiMnO_x$/C electrocatalyst in presence and absence of ethanol at different temperatures. *Black traces*: in pure 1 mol L^{-1} NaOH. *Colored traces*: in the presence of 0.1 mol L^{-1} ethanol

decrease of the value of the ORR current densities is likely due to an effect of deactivation of the catalytic surface by the presence of a small amount of ethanol adsorbed on the catalyst active sites. Other effects, such as superimposition of oxidation currents to the reduction ones (such ethanol oxidation current were indeed not monitored in Fig. 3) or changes in the ORR mechanism are discarded, since it would be reasonable to think that they would have led to more drastic changes in the current densities. Here, it is important to note that the manifested ethanol tolerance of the $NiMnO_x$/C electrocatalyst is even "higher" than that monitored with respect to $NaBH_4$: Even the presence of small amount of Ni phase in addition to $NiMnO_x$ does not seem to yield any consequent ethanol oxidation/adsorption activity, a scenario which was not as favorable in the presence of $NaBH_4$ [17].

In summary, the results obtained in these fundamental studies reveal the apparent suitability of this material as an ethanol-tolerant catalyst. There was no significant decrease in the oxygen reduction current in the presence of ethanol and no significant change in the number of electrons involved. Furthermore, the catalyst shows no activity for ethanol oxidation or adsorption. As a consequence, this material could be postulated as a promising one for being applied in the cathode of an alkaline DEFC.

Single-Cell Tests

A more conclusive test for defining the suitability of $NiMnO_x$/C as cathode catalyst in an alkaline DEFC was made by applications on a single cell. For this purpose, a PBI membrane was used as electrolyte, taking advantage of its amphoteric nature. Indeed, this material has been already applied for alkaline DEFC with satisfactory results [38–41]. Figure 5 shows (current density versus cell voltage) and (power density versus cell voltage) curves of the fuel cell fed with 3 mol L^{-1} KOH and 2 mol L^{-1} ethanol at different temperatures, for anodes formed by PtRu/C and cathodes composed by Pt/C [Fig. 5(a)] (standard material) and $NiMnO_x$/C [Fig. 5b].

All the polarization curves display the three classical regions: activation, ohmic, and mass-transport polarizations. Significant activation losses are present for both electrode systems, which can be an indication of the limited ethanol oxidation kinetics, added to the well-known kinetic limitation of the ORR, overall resulting in high value of Tafel slope. Indeed, for Pt-based catalysts, values of 300 mV dec^{-1} have been reported in alkaline medium for alkaline DEFC [42, 43]. The ohmic polarization region shows a relatively low decay in the cell performance, evidencing a satisfactory conductivity of the KOH impregnated PBI membrane [44]. Finally, significant mass-transport limitations appear in both cases. Some possible reasons of this behavior are the inadequate structure of the electrode for this type of cells, reduction of the effective KOH concentration in the anolyte/electrolyte by formation of carbonates, and also some ethanol adsorption on the cathode material at low cathode potential. Particularly, the used GDE

Table 2 Number of electrons involved in the oxygen reduction reaction (n) and limiting current density (i_{lim}) at 1,600 rpm in the presence and absence of 0.1 mol L^{-1} of ethanol for $NiMnO_x/C$ at different temperatures (values were also calculated for Pt/C as reference)

Temperature/°C	N			$10^3 \cdot j_{lim}$ at 1,600 rpm/mA cm^{-2}	
	Pt/C (reference)	Absence of ethanol	Presence of ethanol	Absence of ethanol	Presence of ethanol
25	4.0	3.1	2.9	−1.85	−1.80
40	4.0	2.9	2.7	−2.31	−2.22
60	3.5	2.6	2.4	−2.48	−2.10

are designed for H_2-based PEMFC and, to a lower extent, non-alkaline liquid DEFC. Paying attention to this latter case, the GDE manages organic products: ethanol, acetaldehyde, acid acetic, ethyl acetate, and carbon dioxide [45–47]. Nevertheless, our highly hydrophobic GDE may not manage so effectively the salts formed in the ethanol oxidation (potassium carbonate and acetate), leading to the significant mass-transport limitations here observed.

In order to better visualize the difference in the performance of both materials, the values of the open circuit voltage (OCV) and the maximum power densities are depicted as a function of temperature in Fig. 6. As it can be observed, the OCVs are higher in the case of Pt/C compared with $NiMnO_x/C$, especially at the lower temperatures. This can be attributed to the intrinsically greater activity for the ORR (especially higher exchange current density) of the noble metal, as already reported [33, 36]. Nevertheless, the OCV values observed for the $NiMnO_x/C$ are quite close to those of Pt/C, particularly at the higher temperatures, demonstrating that this material indeed possesses a good ethanol tolerance, even at high temperature. The values of the maximum power density show a similar behavior than the OCV, with lower values for the NiMnOx/C catalyst, especially at the lower temperatures. This result again shows a (slightly) higher activity of the Pt/C catalyst compared with the $NiMnO_x/C$. However, the difference reduces at higher temperatures, with a maximum power density of 55 mW cm^{-2} for the $NiMnO_x/C$ and 62 mW cm^{-2} for the Pt/C at 90 °C.

A comparison with similar systems could be of interest. In this sense, Hou et al. [48] showed a power peak of 13 mW cm^{-2} for a very similar system based on a quaternized PBI membrane (*N*-ethyl-polybenzimidazole), 2 mg cm^{-2} of 45 % PtRu/C in the anode, and 1 mg cm^{-2} of MnO_2/C in the cathode, operating at 130 °C with air as comburent. Natural diffusion and convection were the feed mechanism for the anode and the cathode,

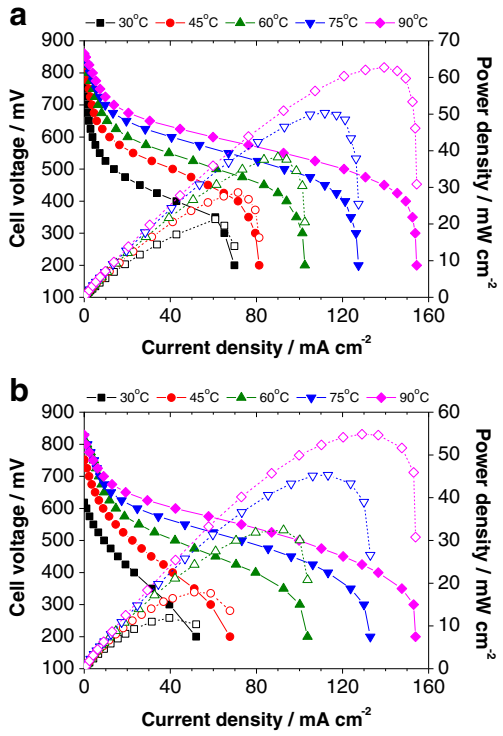

Fig. 5 Cell potential and Power density versus current densities for alkaline single cells operating at different temperatures for the different cathode materials: **a** Pt/C and **b** $NiMnO_x/C$

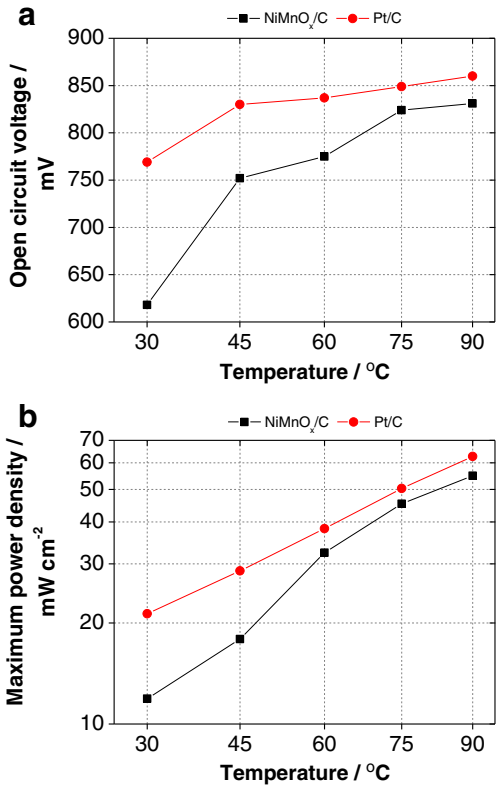

Fig. 6 **a** Open circuit voltage and **b** fuel cell maximum power density for the different cathode catalyst materials at the studied temperatures

respectively. At 60 °C, Hou et al. [39] reported a power peak for this system of 30 mW cm^{-2}. Modestov et al. [38] achieved a maximum power density of 100 mW cm^{-2} at a cell voltage of 0.4 V by using a RuV/C anode catalyst (4.5 mg cm^{-2}) and a cathode of 5,10,15,20-tetrakis(4-methoxyphenyl)-21H,23H-porphine cobalt(II) (TMPhP Co) (9.2 mg cm^{-2}) at 80 °C, with air as oxidant and 3 mol L^{-1} KOH and 2 mol L^{-1} of ethanol as fuel and a PBI-based membrane. Finally, in their early study, Hou et al. [39] reported a power peak of 61 mW cm^{-2} for a 2 mg cm^{-2} PtRu/C anode catalyst, and 1 mg cm^{-2} for a Pt/C cathode catalysts at 90 °C, operating with 2 mol L^{-1} KOH and 2 mol L^{-1} ethanol and with oxygen (absolute pressure of 0.2 MPa) in the cathode.

The fuel cell results obtained here on alkaline PBI-based systems are rather important and significant, since they confirmed the suitability of $NiMnO_x$/C as cathode material for alkaline direct ethanol fuel cells. Clear advantages can be envisaged for its implementation, derived from its non-noble nature: greater availability and lower costs. Nevertheless, some issues still have to be addressed, especially in terms of the durability of this material for long-term applications. Such aspects, studied in the past on a short-term basis in RDE configuration [49], are already being studied in ongoing research activities. Also, another attractive possible application for this material could be in microbial fuel cell systems, in the search for a non-Pt-based cathode. Finally, better results may be expected from a more appropriate design of the GDE that accounts for the particular environment of alkaline ethanol fuel cells, where salts are obtained as the main oxidation products, with a reduced solubility, further limited under the high ionic strength medium used. Also, Pt-based (PtRu/C used in this study) anodes are not the most suitable material for ethanol oxidation in alkaline medium, as recently reviewed by Brouzgou et al. [50].

Conclusions

$NiMnO_x$/C has emerged as a suitable material for ethanol-tolerant cathodes. From a simple synthesis procedure, it is possible to obtain a material which consists of a combination of Ni/NiO/MnO/Mn_2O_3/MnO_2 in the form of nano-structured needles deposited on the carbon support. Although it does not reduce the oxygen molecule in a four-electron pathway, this material has shown a significant oxygen reduction activity that remains immutable despite the presence of ethanol, due to the absence of activity for ethanol oxidation. When applied in a single cell and compared with the standard material Pt/C, $NiMnO_x$/C displays a satisfactory performance, assessed from the slightly lower open circuit voltage and maximum power density. As a consequence, $NiMnO_x$/C can be postulated as a suitable material for alkaline DEFC.

Acknowledgments The Authors thank process n. 2010/07108-3 São Paulo Research Foundation (FAPESP), *Conselho Nacional de Desenvolvimento Científico e Tecnológico* (CNPq), and *Coordenação de Aperfeiçoamento de Pessoal de Nível Superior* (CAPES/COFECUB-Ph 598/08 project) for financial supports. In particular, José J. Linares thanks FAPESP for a post-doctoral fellowship (Proc. 2010/07108-3). Funding by French National Research Agency (ANR) and German Federal Ministry for Education and Research (BMBF) through the Project "Efficient Use of Bio-ethanol in Fuel Cells (EUBECELL) as part of the "Program Inter Carnot Fraunhofer (PICF)" is also gratefully acknowledged.

References

1. K. Kinoshita, *Electrochemical oxygen technology* (Willey, New York, 1992)
2. T.R. Ralph, M.P. Hogarth, Platin Met. Rev. **3**, 46 (2002)
3. R. Parsons, T. VanderNoot, J. Electroanal. Chem. **9**, 257 (1998)
4. A.M. Castro Luna, A. Bonesi, W.E. Triaca, A. Di Blasi, A. Stassi, V. Baglio, V. Antonucci, A.S. Aricò, J Nanoparticle Res. **12**, 357 (2010)
5. A. Kuver, W. Vielstich, J. Power, Sources **74**, 211 (1998)
6. V.A. Sethuraman, J.W. Weidner, A.T. Haug, L.V. Protsailo, J. Electrochem. Soc. **155**, B119 (2008)
7. D.E. Curtin, R.D. Lousenberg, T.J. Henry, P.C. Tangeman, M.E. Tisack, J. Power, Sources **131**, 41 (2004)
8. W. Li, W. Zhou, H. Li, Z. Zhou, B. Zhou, G. Sun, Q. Xin, Electochim. Acta **49**, 1045 (2004)
9. K. Ramya, K.S. Dhathathreyan, J. Electroanal. Chem. **542**, 109 (2003)
10. J. Lobato, P. Cañizares, M.A. Rodrigo, J.J. Linares, Electrochim. Acta **52**, 3910 (2007)
11. X. Yu, S. Ye, J. Power, Sources **11**, 145 (2007)
12. Y. Sun, M. Delucchi, J. Ogden, Int. J. Hydrogen Energy **36**, 11116 (2011)
13. I. Staffell, R. Green, Int. J. Hydrogen Energy **38**, 1088 (2013)
14. T. Takakuwa, M. Akiyoshi, T. Kenko, M. Saito, H. Daimon, A. Tasaka, M. Inaba, H. Shiroishi, T. Hatai, J. Kuwano, ECS Trans. **41**, 2185 (2011)
15. Q. Wen, S. Wang, J. Yan, L. Cong, Z. Pan, Y. Ren, Z. Fan, J. Power, Sources **216**, 187 (2012)
16. R.B. Valim, M.C. Santos, M.R.V. Lanza, S.A.S. Machado, F.H.B. Lima, M.L. Calegaro, Electrochim. Acta **85**, 423 (2012)
17. A.C. Garcia, F.H.B. Lima, E.A. Ticianelli, M. Chatenet, J. Power, Sources **222**, 305 (2013)
18. P. Bezdicka, T. Grygar, B. Klápste, J. Vondrák, Electrochim. Acta **45**, 913 (1999)
19. A.C. Garcia, A.D. Herrera, E.A. Ticianelli, M. Chatenet, C. Poinsignon, J. Electrochem. Soc. **158**, B290 (2011)
20. J.P. Hoare, *The electrochemistry of oxygen* (John Wiley & Sons, New York, 1968), p. 19
21. A.J. Bard, L.R. Faulkner, *Electrochimie—Principles* (Méthodes et Applications, Masson, Paris, 1983)
22. L.F. Hiemke, The influence of reactant gas solubility on flooded fuel cells. B. Sc. Thesis, MIT, 1991
23. M. Chatenet, M. Aurousseau, R. Durand, Electrochim. Acta **45**, 2823 (2000)
24. M. Chatenet, M. Aurousseau, R. Durand, Comparative methods for gas diffusivity and solubility determination in extreme media: Application to molecular oxygen in an industrial chlorine-soda electrolyte. Ind. Eng. Chem. Res. **39**, 3083 (2000)
25. P. Han, D.M. Bartels, J. Phys. Chem. **100**, 5597 (1996)
26. M. Chatenet, M.B. Molina-Concha, N. El-Kissi, G. Parrour, J.-P. Diard, Direct rotating ring-disk measurement of the sodium borohydride diffusion coefficient in sodium hydroxide solutions. Electrochim. Acta **54**, 4426 (2009)
27. W.H. Baur, Acta Crystallogr. B **32**, 2200 (1976)

28. S. Geller, Acta Crystallogr. B **27**, 821 (1971)
29. S. Sasaki, K. Fujino, Y. Takeuchi, Proc. Jpn Acad. **55**, 43 (1979)
30. M. Yousug, P.C. Sahy, H.K. Jajoo, S. Rajagopalan, K. Govinda Rajan, J. Phys. F **16**, 373 (1986)
31. L. Li, K. Scott, E.H. Yu, J. Power, Sources **221**, 1 (2013)
32. Y. Zhang, Y. Hu, S. Li, J. Sun, B. Hou, J. Power, Sources **22**, 9284 (2011)
33. I. Roche, E. Chainet, M. Chatenet, J. Vondrák, J. Phys. Chem. C **111**, 1434 (2007)
34. F.H.B. Lima, M.L. Calegaro, E.A. Ticianelli, J. Electroanal. Chem. **590**, 152 (2006)
35. J. Vondràk, B. Klápště, J. Velická, M. Sedlaříková, V. Novàk, J. Reiter, J New Mater. Electrochem. Syst. **8**, 1 (2005)
36. I. Roche, K. Scott, J. Electroanal. Chem. **638**, 280 (2010)
37. K. Kinoshita, *Carbon, electrochemical and physicochemical properties* (John Wiley & Sons, New York, 1988)
38. A.D. Modestov, M.R. Tarasevich, A.Y. Leykin, V. Ya, Filimonov. J. Power. Sources **188**, 502 (2009)
39. H. Hou, G. Sun, R. He, Z. Wu, B. Sun, J. Power, Sources **182**, 95 (2008)
40. H. Hou, S. Wang, Q. Jiang, W. Jin, L. Jiang, G. Sun, J. Power. Sources **196**, 3244 (2011)
41. L. An, T.S. Zhao, Q.X. Wu, L. Zeng, Int. J. Hydrogen Energy **37**, 14536 (2012)
42. L. Ma, D. Chu, R. Chen, Int. J. Hydrogen Energy **37**, 11185 (2012)
43. L. Jiang, A. Hsu, D. Chu, R. Chen, Int. J. Hydrogen Energy **35**, 365 (2010)
44. H. Hou, G. Sun, R. He, B. Sun, W. Jin, H. Liu, Q. Xin, Int. J. Hydrogen Energy **33**, 7172 (2008)
45. F. Colmati, E. Antolini, E.R. Gonzalez, J. Power, Sources **157**, 98 (2006)
46. J.J. Linares, T.A. Rocha, S. Zignani, V.A. Paganin, E.R. Gonzalez, Int. J. Hydrogen Energy **38**, 620 (2013)
47. V.A. Paganin, E.A. Ticianelli, E.R. Gonzalez, J. Appl. Electrochem. **26**, 297 (1996)
48. H. Hou, S. Wang, H. Liu, L. Sun, W. Jin, M. Jing, L. Jiang, G. Sun, Int. J. Hydrogen Energy **36**, 11955 (2011)
49. I. Roche, E. Chainet, J. Vondrak, M. Chatenet, J. Appl. Electrochem. **38**, 1195 (2008)
50. A. Brouzgou, A. Podias, P. Tsiakaras, J. Appl. Electrochem. **43**, 119 (2013)